Energy & Environmental Science

COMMUNICATION

View Article Online
View Journal

N-doped graphitic self-encapsulation for high performance silicon anodes in lithium-ion batteries†

Cite this: DOI: 10.1039/c3ee43322f

Received 6th October 2013
Accepted 30th October 2013

DOI: 10.1039/c3ee43322f

www.rsc.org/ees

Won Jun Lee,[ab] Tae Hoon Hwang,[c] Jin Ok Hwang,[ab] Hyun Wook Kim,[d] Joonwon Lim,[ab] Hu Young Jeong,[e] Jongwon Shim,[ab] Tae Hee Han,[f] Je Young Kim,[d] Jang Wook Choi*[c] and Sang Ouk Kim*[ab]

N-doped sites at CNT and graphene trigger spontaneous encapsulation of Si particles by simple pH control at room temperature. Significantly, N-doped CNT encapsulated Si composite electrode materials show remarkable cycle life and rate performance in battery operations. Superior capacity retention of 79.4% is obtained after 200 cycles and excellent rate capability of 914 mA h g^{-1} is observed at a 10 C rate.

Broader context

Silicon (Si) anodes are a promising candidate as an alternative to conventional graphitic anodes in lithium-ion batteries (LIBs), with an unparalleled theoretical capacity near to 4000 mA h g^{-1}. Unfortunately, Si anodes generally suffer from significant volume changes upon lithiation, which frequently results in their pulverization and disintegration. In this regard, integration of Si with graphitic carbon nanomaterials has been considered to be a promising approach. However, such carbon integration usually requires complicated processing steps and high temperature treatment, making overall synthetic procedures less scalable. The present study demonstrates a straightforward route to high performance Si-based anodes by engaging N-doped graphitic carbon encapsulants (N-doped CNTs and graphene). The N-doped sites at the graphitic carbon surface trigger spontaneous and rapid encapsulation of commercial Si particles *via* simple surface charge tuning with pH control. The overall procedure was performed under mild conditions of room temperature, ambient pressure, and aqueous media with a reaction time of less than 30 min. This is the first observation of spontaneous integration of carbon materials over a Si particle surface without high temperature treatment or any other pre-treatment.

Lithium-ion batteries (LIBs) have been successful in powering a variety of portable electronic devices in virtue of their high energy densities and reasonably long lifetime.[1–4] Nevertheless, emerging large-scale applications represented by hybrid electrical vehicles (EVs), stationary grid energy storage systems, and advanced portable electronics are imposing more challenging standards with regard to various cell aspects. In particular, the simultaneous increase in the energy density and cycle life are a crucial requirement for those new LIB applications.[5] For instance, in EV applications, the energy density and cycle life are directly associated with driving distance per charge and lifetime, respectively.

Silicon (Si) anodes have received a great deal of attention due to their unparalleled theoretical capacity near to 4000 mA h g^{-1},[6–9] which is more than 10 times larger than that of conventional graphite anodes (~372 mA h g^{-1}). Additionally, Si is abundant in the Earth's crust and environmentally benign. Nonetheless, most Si anodes suffer from limited cycle life, which stems from significant volume expansion (up to ~400%) upon full lithiation.[10] Such a large volume change causes several severe fading mechanisms, including pulverization of the active material, contact loss with conductive carbon agents, and unstable solid electrolyte interphase (SEI) formation. In this regard, integration of nanostructured Si with carbon (C) nanomaterials in the porous electrodes has been considered as one of the most promising approaches.[1,11–15] In this composite structure, (1) the void space accommodates the volume expansion of Si,[16] (2) the carbon nanomaterials compensate for the low electronic conductivity of intrinsic Si,[17] and (3) the overall electrode structure is allowed to maintain stable SEI layers formed on the carbon surfaces.

We have developed Si/C composite LIB anodes by engaging N-doped graphitic carbon encapsulants. The N-doping plays a critical role in the straightforward self-encapsulation of carbon nanotubes (CNTs) and graphene at the bare Si particle surface

[a]Center for Nanomaterials and Chemical Reactions, Institute for Basic Science (IBS), Daejeon 305-701, Korea
[b]Materials Science & Engineering, KAIST, Daejeon 305-701, Korea. E-mail: sangouk.kim@kaist.ac.kr
[c]Graduate School of EEWS (WCU), KAIST Institute NanoCentury, KAIST, Daejeon 305-701, Korea. E-mail: jangwookchoi@kaist.ac.kr
[d]Battery R&D, LG Chem, Ltd, 104-1 Moonji-dong, Yuseong-gu, Daejeon 305-380, Korea
[e]UNIST Central Research Facility and School of Mechanical and Advanced Materials Engineering, UNIST, Ulsan 689-798, Korea
[f]Department of Organic and Nano Engineering, Hanyang University, Seoul 133-791, Korea

† Electronic supplementary information (ESI) available: TEM, SEM, XPS, EDS, workfunction, electrochemical properties of various C/Si composites. See DOI: 10.1039/c3ee43322f

without any pre- or post-treatment.[18,19] The resultant electrochemical performance of Si based anodes demonstrated remarkable enhancement, especially in terms of cycle life and rate performance. The overall procedures were based on mild conditions of ambient pressure, low temperature, and aqueous media, which is clearly in contrast with currently available counterparts requiring high temperature processing steps.[11,20,21]

Our graphitic self-encapsulation is schematically illustrated in Fig. 1a. The encapsulation was achieved by simple mixing of aqueous dispersions including Si and N-doped carbons. This process does not require high temperature treatment for close Si–C contacts, and is thus energy efficient and environmentally benign.[18,19] The generality of the approach was assured by employing commercially available Si particles with a wide range of diameters (50–200 nm, Sigma Aldrich, US, see Fig. 1b). High resolution transmission electron microscope (HRTEM, see Fig. 1c) characterization confirms ~3 nm thick native Si oxide layers at Si particle surfaces. X-ray photoemission spectroscopy (XPS) supports the presence of the SiO_2 layers (see Fig. S1a, ESI†, inset), as the Si 2p spectrum shows two peaks corresponding to both Si and SiO_2. These SiO_2 oxide layers play a critical role in the electrostatic interaction with graphitic carbon materials. It is well known that the oxide surface of the silicon would become strongly negatively charged above pH 7 due to deprotonation of the silanol (SiOH) groups.[22,23] The negative surface charge density due to these SiO^- groups easily attracts the counterparts having a positively charged surface that can take part in electrostatic interaction.

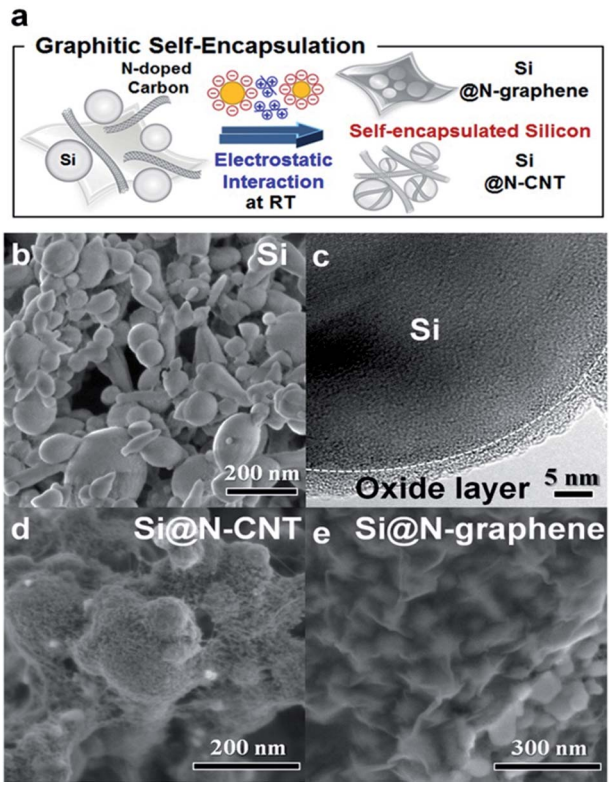

Fig. 1 Graphitic self-encapsulation of Si with N-doped graphitic carbons. (a) A schematic illustration of graphitic self-encapsulation. Mixing pH was controlled for electrostatic attraction between the SiO_2 surface and N-doped sites at graphitic carbons. (b) HR-SEM and (c) HR-TEM images of Si particles. The surface SiO_2 layer is indicated. HR-SEM images of (d) N-CNT encapsulated Si particles and (e) N-graphene encapsulated Si particles.

Two forms of N-doped graphitic encapsulants were employed in this work: two-dimensional (2D) N-doped graphene (N-doping concentration: 8.34 at%) and one-dimensional (1D) N-doped carbon nanotubes (CNTs) (N-doping concentration: 3.56 at%) (see Fig. S1b–e, ESI†). The difference in N-doping concentrations resulted from their different synthesis procedures (hydrazine treatment for graphene *vs.* ammonia treatment for CNTs) (see ESI†, Experimental section).[24] The N-doping of graphitic carbons has been exploited for various applications thus far.[25–28] N-doping can manipulate the local electronic structures and eventually modify the overall properties of graphitic carbons, including morphology, electrical resistance, and workfunction (Table S1, ESI†).[18,29–32] More significantly, N-doping facilitates solution dispersion and also allows the control of surface energy and charge states. N-dopants having a higher electronegativity than carbon facilitate permanent dipoles at neutral graphitic surfaces such that surface energy can be greatly enhanced. Nitrogen, with lone pair electrons, can also be protonated and deprotonated by pH control for surface charge tunability. These features are crucial for the self-encapsulation in this work. XPS analyses reveal two types of N-doped sites: pyridinic N (N_P), and quaternary N (N_Q) (see Fig. S1b and S1e, ESI†). Fig. S1b, ESI† illustrates the atomic configurations of the N-doped sites. Both types of N-sites are active for the surface charge tuning with pH control.[33] Hereafter, we denote N-doped CNT encapsulated Si and N-doped graphene encapsulated Si as Si@N-CNT and Si@N-graphene, respectively, for convenience.

Fig. 1d and e show the encapsulated morphologies of N-doped graphitic carbons around Si particles characterized by ultrahigh resolution scanning electron microscopy (UHR-SEM) with a low acceleration voltage (500 V). Both CNT and graphene yielded densely encapsulated interconnected structures. Remarkably, even for a large size distribution of Si particles, each N-doped graphitic encapsulant showed an excellent ability to encapsulate Si particles regardless of their size. While N-graphene flakes seal Si particles with their two dimensional, large size, N-CNTs show web-like encapsulation behavior towards each Si particle, employing their wire characteristics. This morphological difference leads to a significant change in the battery application, as discussed below. The spontaneous encapsulation behavior was monitored as a function of mixing time (see Fig. S1f, ESI†). While the TEM image taken immediately after the mixing of two dispersions shows thin carbon layers on SiO_2 surfaces, the one taken after 30 min of mild stirring (at room temperature) shows thicker and uniform encapsulation. Under the optimal encapsulation conditions, the dark mixing solution becomes transparent, indicating that the majority of graphitic carbons participate in the encapsulation. Elemental line scan profiles (see Fig. S1g, ESI†) support the uniformity of encapsulation around Si particles.

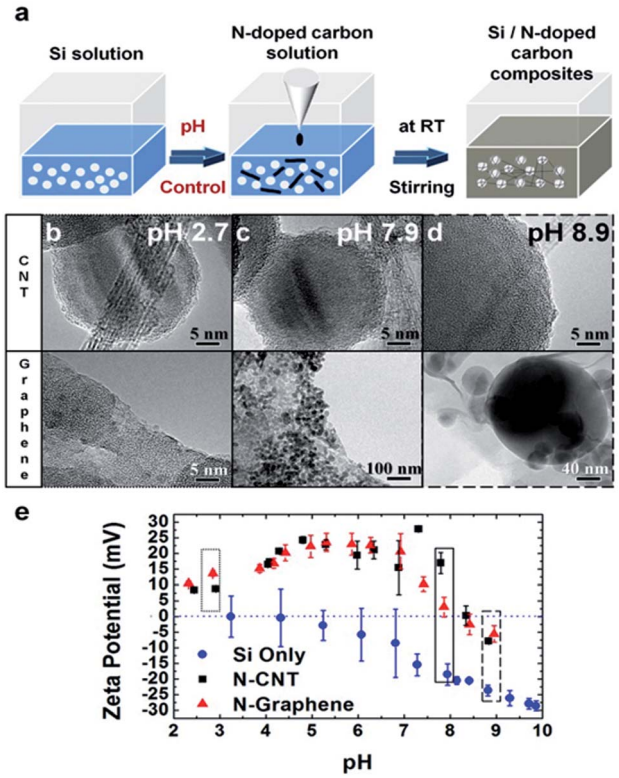

Fig. 2 Electrostatic interaction between N-doped carbons and Si. (a) Experimental procedure for graphitic self-encapsulation of Si particles. TEM images of Si encapsulated with N-CNTs (top) and N-graphene (bottom) at pH values of (b) 2.7, (c) 7.9, and (d) 8.9. (e) Zeta-potential measurements of Si particles, N-CNTs, and N-graphene at various pH values.

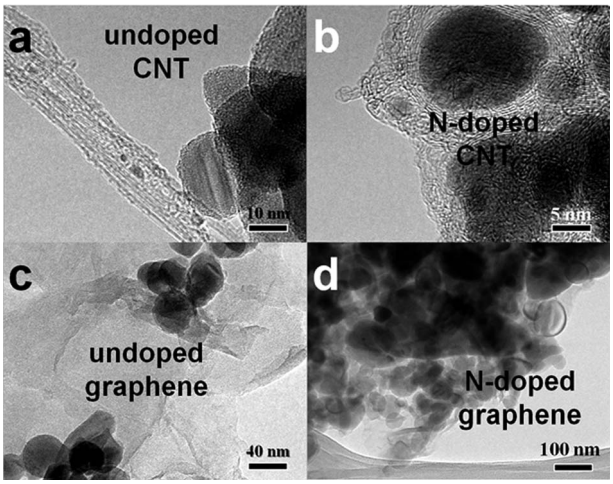

Fig. 3 N-doping for self-encapsulation of Si particles. TEM images of encapsulation with (a) undoped CNT, (b) N-doped CNT, (c) undoped graphene, and (d) N-doped graphene.

The self-encapsulation was further elucidated and optimized, focusing on pH control,[34] as illustrated in Fig. 2a.[35,36] The pH values of 2.7, 7.9, and 8.9 were tested, and their respective TEM images are presented in Fig. 2b–d. Among the tested conditions, only pH = 7.9 exhibits uniform encapsulation, while the others result in bare and nonuniform encapsulation. This morphological variation can be understood by the surface charge governed by the pH of the mixing solution. Fig. 2e compares the zeta potentials of Si and N-doped graphitic carbons. The zeta potential of Si largely fluctuates at pH < 7.0 but persistently maintains negative values above 7.0, which is consistent with the results reporting the isoelectric point of silicon oxide.[21] This fluctuation under low pH conditions is attributed to unstable proton interactions with the hydroxyl groups on the silica surfaces. For graphitic carbons, positive zeta potentials at low pH conditions cross over to negative values around pH = 8.5, which is the isoelectric point of N-doped graphitic carbons.[37] Consequently, pH 7.9, Si and N-doped carbon materials are oppositely charged, leading to spontaneous electrostatic attraction.

As a control test to confirm the role of N-doping for attractive interactions, the same experiments were repeated with undoped carbon materials. Both undoped CNTs and graphene suffered from poor aqueous dispersion due to their hydrophobic nature, and revealed far inferior encapsulating capabilities (see Fig. 3). The morphologies of graphitic encapsulated Si particles were characterized further in bulk powder and films. As shown in Fig. S2a–c, ESI,† the pure Si without encapsulation exhibits dense packing, whereas Si@N-CNT exhibits secondary porous structures on the scale of several hundreds of nanometers. This porosity results from the N-CNT skeletal backbones that cause the agglomeration of Si particles along their lengths. By contrast, Si@N-graphene shows highly dense packing (see Fig. S2c, ESI†), due to the large flake sizes and flexible 2D geometry of graphene, which could be effective in connecting between Si particles. Such inter-particle connection through graphene layers generates mesopores (2–50 nm). However, it is well-known that micropores (<2 nm) also exist in this sample from the intrinsic defects within N-graphene flakes.[38] More detailed porosity data is given below.

Electrical conductivities of the three kinds of electrodes prepared were characterized employing a four-point method (see Fig. S2d, ESI†). As shown in Fig. S2e, ESI,† the pure Si electrode exhibits a low conductivity due to the semiconducting nature of intrinsic Si. Owing to the electrically conductive N-doped graphitic carbons, the encapsulated ones show substantially higher conductivities. Specifically, the sheet resistance of Si@N-graphene was approximately two times smaller than that of Si@N-CNT. The 2D graphene readily builds up abundant conductive pathways within the electrode. The porosities of electrode samples were characterized by N_2 adsorption–desorption, as presented in Fig. S2f, ESI.† Brunauer–Emmett–Teller (BET) surface areas of pure Si, Si@N-CNT, and Si@N-graphene were 30.5, 51.7, and 79.5 $m^2\ g^{-1}$, respectively. The large surface areas of both encapsulated electrodes are due to the intrinsic large surface areas of graphitic carbons. Consistently, the fact that the specific surface area of Si@N-graphene is larger than that of Si@N-CNT is attributed to the larger surface area of graphene. Based on the isotherms, the BJH pore size distributions were obtained (see Fig. S2g, ESI†). The results indicate that the graphitic

self-encapsulation leads to the formation of mesopores (2–50 nm), which should be attributed to the network formation of graphitic carbons. The sheet resistances, BET areas, and average pore sizes of three electrodes are summarized in Fig. S2h, ESI.† The mass composition of graphitic carbon self-encapsulated Si was analysed with thermogravimetric analysis (TGA) (see Fig. S3, ESI†).

The electrochemical performances of the three electrodes were characterized in coin-type half-cells (see Experimental section, ESI†). Galvanostatic mode was employed in the potential range of 0.01–1.2 V (*versus* Li^+/Li). Lithium foil was used for reference and counter electrodes simultaneously. The working electrode consists of 70 wt% of active material including carbon encapsulants, 15 wt% of super P, and 15 wt% of poly(acrylic acid) (PAA) binder. The active material loading density was ~0.8 mg cm^{-2}. To confirm the effectiveness of our graphitic self-encapsulation method, the electrochemical performance of Si@N-CNT was comparatively tested against various other samples including Si@N-graphene, Si/N-CNT blend, Si/undoped CNT, and Si/undoped graphene. Significantly, Si@N-CNT exhibits the best performance among them (see Fig. S4, ESI†). Fig. 4a shows potential profiles during the first cycles measured at a current density of 100 mA g^{-1}. We note that, if not indicated, all the C-rates addressed in this work correspond to 1 C values (1265 mA g^{-1} for Si@N-CNT, and 2647 mA g^{-1} for Si only), which are different from practical charge–discharge durations.

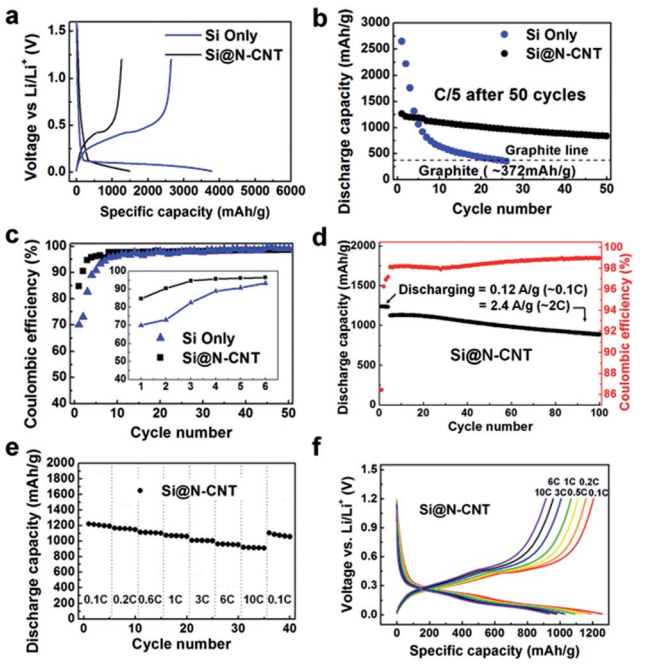

Fig. 4 Electrochemical characterization of pure and graphitic encapsulated Si anodes. (a) Potential profiles of pure Si and Si@N-CNT during the first cycles at a C/10 rate. (b) Reversible discharge capacities and (c) coulombic efficiencies during 50 cycles. (d) Cycling performance of Si@N-CNT measured at 2 C. (e) Rate capability tests for Si@N-CNT at various C-rates. (f) Galvanostatic charge–discharge profiles of Si@N-CNT in the C-rate of C/10–10 C. The gravimetric capacities are normalized with the total mass of Si and N-doped CNT encapsulant.

All samples show the characteristic charge and discharge plateaus of Si at 0.1 and 0.4 V *versus* Li/Li^+, respectively. Si@N-CNT exhibits the best reversibility, as it delivers 1493 and 1265 mA h g^{-1} for the charge (lithiation) and discharge (delithiation), respectively. This leads to the first coulombic efficiency (CE) of 84.8%. By contrast, pure Si shows 3782 and 2647 mA h g^{-1}, respectively, with a CE of 70%, which is consistent with literature values.[10,39] It is noteworthy that the first CE of Si@N-CNT is comparable to the highest value of a Si anode system ever reported thus far.[40,41] The CNT layers thoroughly cover the Si surface and form stable SEI layers, whose electrochemical reversibility is much better than those at the bare Si surface.

The capacity retentions measured at C/5 for both charge and discharge and corresponding CEs are presented in Fig. 4b and c, respectively. Apparently, the pure Si electrode exhibits abrupt capacity decay within 20 cycles, presumably due to the well-known intrinsic issues, including contact loss with super P and unstable SEI formation.[42] After 50 cycles, Si@N-CNT shows 838.2 mA h g^{-1} with capacity retention of 74.4% from the initial values. In terms of CE, Si@N-CNT exhibits the highest values in the early cycles, indicating stable SEI formation. The relatively more serious capacity decay in the beginning period could be critical for future full-cell operations and could be addressed by development of electrolyte additives and binders as well as further cell optimization such as hot-pressing of electrodes. Notably, even after 100 cycles at a higher discharge rate of 2 C, specific capacity of 941.7 mA h g^{-1} is obtained with retention of 79.4% and a CE of 99.4% (see Fig. 4d). Also, a simple N-CNT/Si blend shows far inferior capacity retention (see Fig. S5, ESI†), reconfirming the importance of encapsulation of N-CNTs for the cycling performance. Furthermore, Si@N-CNT demonstrates excellent rate capability (see Fig. 4e and f). When the C-rate sequentially increases from C/10 (= 0.12 A g^{-1}) to 1 C (= 1.2 A g^{-1}) to 10 C (= 12.1 A g^{-1}), good capacity retention is maintained, as the specific capacity varies from 1205 mA h g^{-1} to 1068 mA h g^{-1} to 914 mA h g^{-1}, respectively.

The electrochemical performance of Si@N-graphene was also characterized (see Fig. S6, ESI†). While the encapsulation of N-graphene results in improved cell performance, the reversibility of Si@N-graphene is inferior to that of Si@N-CNT due mainly to functional groups at the edges of graphene that could cause irreversible binding with Li ions. Previously, Park *et al.* reported the preferential formation of pyrazole functional groups at the edges of graphene upon hydrazine treatment.[43] It has been found that pyrazole groups form stable complexes with alkali metals such as Li, Na, and K.[44] Thus, it is expected in our case that the –NH and =N groups in the pyrazole groups strongly bind with Li ions and therefore contribute to the irreversible nature of Si@N-graphene.

The morphology variation of composite electrodes was characterized after cycling (see Fig. 5a and Fig. S7, ESI†), as shown in Fig. 5b and c. After 100 cycles, Si@N-CNT maintains the initial morphology that Si particles are well-encapsulated with N-CNTs, while some N-CNT bridges among Si particles. Such a high stability is largely owing to the high rigidity of the bundled N-CNT network structure, well-maintained even after

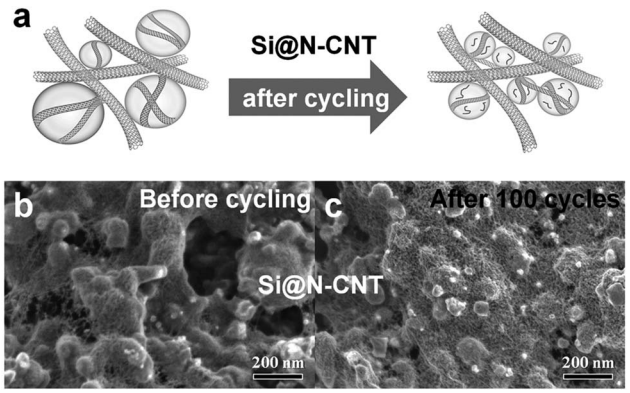

Fig. 5 Electrode morphology change before and after cycling. (a) Schematic illustration of electrode morphology change. HR-SEM images of Si@N-CNT (b) before and (c) after 100 cycles at 1 C.

repeated severe volume changes during battery operation. It demonstrates that the robustness of the carbon encapsulant structure is crucial for the stable performance of composite electrode materials. Overall, the superior cycling performance of Si@N-CNT is associated with the stable interaction between N-CNTs and Si particles, which guarantees efficient electron transport as well as formation of stable SEI layers during cycling.

Conclusions

We have demonstrated spontaneous room temperature graphitic encapsulation of Si particles for high performance LIB anodes with two different graphitic carbons (CNT and graphene). Unlike other carbonization processes, generally requiring high temperature treatments, our approach utilizes the straightforward electrostatic interactions between N-doped sites of graphitic carbons and surface hydroxyl functionalities of Si for effective encapsulation *via* solution mixing. The overall procedure is performed at room temperature, in mild aqueous media, and at ambient pressure. Between both N-doped carbon encapsulated cases, Si@N-CNT exhibits superior battery performance, especially in terms of cycle life and rate capability. Our N-doped graphitic self-encapsulation is quite versatile and potentially useful for other alloy-based electrode materials, which commonly suffer from large volume changes during electrochemical operation.

Acknowledgements

This work was principally supported by the Institute for Basic Science (IBS) (CA1301-2) and Converging Research Program through the Korea government (MEST) (2012K001260). J. W. C. acknowledges a grant from the National Research Foundation of Korea (NRF) (NRF-2012-R1A2A1A01011970).

Notes and references

1 J. M. Tarascon and M. Armand, *Nature*, 2001, **414**, 359–367.
2 M. Armand and J. M. Tarascon, *Nature*, 2008, **451**, 652–657.
3 J. B. Goodenough and Y. Kim, *Chem. Mater.*, 2010, **22**, 587–603.
4 M. S. Whittingham, *Chem. Rev.*, 2004, **104**, 4271–4301.
5 *2008 Annual Progress Report for the Energy Storage Research and Development Vehicle Technologies Program*, U. S. Department of Energy, Washington DC, 2008.
6 U. Kasavajjula, C. Wang and A. J. Appleby, *J. Power Sources*, 2007, **163**, 1003–1039.
7 J. P. Maranchi, A. F. Hepp and P. N. Kumta, *Electrochem. Solid-State Lett.*, 2003, **6**, A198.
8 T. D. Hatchard and J. R. Dahn, *J. Electrochem. Soc.*, 2004, **151**, A838.
9 C. K. Chan, H. Peng, G. Liu, K. McIlwrath, X. F. Zhang, R. A. Huggins and Y. Cui, *Nat. Nanotechnol.*, 2008, **3**, 31–35.
10 H. Kim, B. Han, J. Choo and J. Cho, *Angew. Chem., Int. Ed.*, 2008, **47**, 10151–10154.
11 M.-H. Park, M. G. Kim, J. Joo, K. Kim, J. Kim, S. Ahn, Y. Cui and J. Cho, *Nano Lett.*, 2009, **9**, 3844–3847.
12 Y. Yu, L. Gu, C. Zhu, S. Tsukimoto, P. A. Van Aken and J. Maier, *Adv. Mater.*, 2010, **22**, 2247–2250.
13 J. H. Ryu, J. W. Kim, Y.-E. Sung and S. M. Oh, *Electrochem. Solid-State Lett.*, 2004, **7**, A306.
14 A. Magasinski, P. Dixon, B. Hertzberg, A. Kvit, J. Ayala and G. Yushin, *Nat. Mater.*, 2010, **9**, 353–358.
15 S.-H. Ng, J. Wang, D. Wexler, K. Konstantinov, Z.-P. Guo and H.-K. Liu, *Angew. Chem., Int. Ed.*, 2006, **45**, 6896–6899.
16 J. Luo, X. Zhao, J. Wu, H. D. Jang, H. H. Kung and J. Huang, *J. Phys. Chem. Lett.*, 2012, **3**, 1824–1829.
17 Y. J. Cho, H. S. Kim, H. Im, Y. Myung, G. B. Jung, C. W. Lee, J. Park, M.-H. Park, J. Cho and H. S. Kang, *J. Phys. Chem. C*, 2011, **115**, 9451–9457.
18 W. J. Lee, D. H. Lee, T. H. Han, S. H. Lee, H.-S. Moon, J. A. Lee and S. O. Kim, *Chem. Commun.*, 2011, **47**, 535–537.
19 W. J. Lee, J. M. Lee, S. T. Kochuveedu, T. H. Han, H. Y. Jeong, M. Park, J. M. Yun, J. Kwon, K. No, D. H. Kim and S. O. Kim, *ACS Nano*, 2012, **6**, 935–943.
20 T. Umeno, K. Fukuda, H. Wang, N. Dimov, T. Iwao and M. Yoshio, *Chem. Lett.*, 2001, 1186–1187.
21 Y.-S. Hu, R. Demir-Cakan, M.-M. Titirici, J.-O. Müller, R. Schlögl, M. Antonietti and J. Maier, *Angew. Chem., Int. Ed.*, 2008, **47**, 1645–1649.
22 R. Raiteri, B. Margesin and M. Grattarola, *Sens. Actuators, B*, 1998, **46**, 126–132.
23 H. Chang, F. Kosari, G. Andreadakis, M. A. Alam, G. Vasmatzis and R. Bashir, *Nano Lett.*, 2004, **4**, 1551–1556.
24 U. N. Maiti, W. J. Lee, J. M. Lee, Y. Oh, J. Y. Kim, J. E. Kim, J. Shim, T. H. Han and S. O. Kim, *Adv. Mater.*, 2013, DOI: 10.1002/adma.201303265.
25 K. Gong, F. Du, Z. Xia, M. Durstock and L. Dai, *Science*, 2009, **323**, 760–764.
26 W. H. Shin, H. M. Jeong, B. G. Kim, J. K. Kang and J. W. Choi, *Nano Lett.*, 2012, **12**, 2283–2288.
27 S. K. Hwang, J. M. Lee, S. Kim, J. S. Park, H. I. Park, C. W. Ahn, K. J. Lee, T. Lee and S. O. Kim, *Nano Lett.*, 2012, **12**, 2217–2221.

28 M. Li, W. Wu, W. Ren, H.-M. Cheng, N. Tang, W. Zhong and Y. Du, *Appl. Phys. Lett.*, 2012, **101**, 103107.
29 D. H. Lee, W. J. Lee and S. O. Kim, *Nano Lett.*, 2009, **9**, 1427–1432.
30 J. O. Hwang, J. S. Park, D. S. Choi, J. Y. Kim, S. H. Lee, K. E. Lee, Y.-H. Kim, M. H. Song, S. H. Yoo and S. O. Kim, *ACS Nano*, 2012, **6**, 159–167.
31 D. H. Lee, W. J. Lee, W. J. Lee, S. O. Kim and Y.-H. Kim, *Phys. Rev. Lett.*, 2011, **106**, 175502.
32 S. H. Lee, H. W. Kim, J. O. Hwang, W. J. Lee, J. Kwon, C. W. Bielawski, R. S. Ruoff and S. O. Kim, *Angew. Chem., Int. Ed.*, 2010, **49**, 10084–10088.
33 Y. F. Jia, B. Xiao and K. M. Thomas, *Langmuir*, 2002, **18**, 470–478.
34 S. Ko, J.-I. Lee, H. S. Yang, S. Park and U. Jeong, *Adv. Mater.*, 2012, **24**, 4451–4456.
35 T. H. Han, W. J. Lee, D. H. Lee, J. E. Kim, E.-Y. Choi and S. O. Kim, *Adv. Mater.*, 2010, **22**, 2060–2064.
36 S. Yang, X. Feng, S. Ivanovici and K. Müllen, *Angew. Chem., Int. Ed.*, 2010, **49**, 8408–8411.
37 G. M. K. Abotsi and A. W. Scaroni, *Carbon*, 1990, **28**, 79–84.
38 Y. Zhu, S. Murali, M. D. Stoller, K. J. Ganesh, W. Cai, P. J. Ferreira, A. Pirkle, R. M. Wallace, K. A. Cychosz, M. Thommes, D. Su, E. A. Stach and R. S. Ruoff, *Science*, 2011, **332**, 1537–1541.
39 H. Wu, G. Chan, J. W. Choi, I. Ryu, Y. Yao, M. T. McDowell, S. W. Lee, A. Jackson, Y. Yang, L. Hu and Y. Cui, *Nat. Nanotechnol.*, 2012, **7**, 310–315.
40 W. Wang and P. N. Kumta, *ACS Nano*, 2010, **4**, 2233–2241.
41 T. H. Hwang, Y. M. Lee, B.-S. Kong, J.-S. Seo and J. W. Choi, *Nano Lett.*, 2012, **12**, 802–807.
42 N. Dimov, Y. Xia and M. Yoshio, *J. Power Sources*, 2007, **171**, 886–893.
43 S. Park, Y. Hu, J. O. Hwang, E.-S. Lee, L. B. Casabianca, W. Cai, J. R. Potts, H.-W. Ha, S. Chen, J. Oh, S. O. Kim, Y.-H. Kim, Y. Ishii and R. S. Ruoff, *Nat. Commun.*, 2012, **3**, 638.
44 G. Tarrago, C. Marzin, O. Najimi and V. Pellegrin, *J. Org. Chem.*, 1990, **55**, 420–425.

